CHEMISTRY
A EUROPEAN JOURNAL

FULL PAPER

DOI: 10.1002/chem.201303075

An Iron Impurity in Multiwalled Carbon Nanotube Complexes with Chitosan that Biomimics the Heme-Peroxidase Function

Prakasam Gayathri and Annamalai Senthil Kumar*[a]

Abstract: A new biomimetic functional system having an impure multiwalled carbon nanotube (MWCNT-Fe)–chitosan biopolymer (H_2N–CHIT) chemically modified glassy carbon electrode (GCE/[MWCNT-Fe:H_2N-CHIT]) has been developed and demonstrated efficient hydrogen peroxide electrocatalytic and electrochemical sensing applications in pH 7 phosphate buffer solution (PBS). The hybrid system showed a stable and well-defined surface confined redox peak at an apparent electrode potential, $E^{\circ\prime} = -0.22$ V versus Ag/AgCl with surface excess value 13.63 nmol cm^{-2}. Physicochemical characterizations of the hybrid by using FESEM, TEM, Raman spectroscopy, FTIR, and various control electrochemical experiments revealed that the iron impurity in the MWCNT interacted with the amino functional group of the chitosan polymer and thereby formed an unique complex-like structure ([MWCNT-$Fe^{III/II}$:NH_2-CHIT]), similar to heme peroxidase with a central $Fe^{III/II}$-redox-active site. The biomimetic system followed Michaelis–Menten-type reaction kinetics for the H_2O_2 reduction reaction with a K_M value of 0.23 mM. At pH 7, amperometric *i–t* sensing and flow-injection analysis of H_2O_2 on the biomimetic system showed calibration plots in windows 5–500 and 50–2500 μM, with detection-limit values of 2.3 and 9.7 μM, respectively. Unlike most of the previously reported systems that undergo serious interferences in physiological pH, the biomimetic system displayed a remarkable tolerance to other co-existing interferants (such as cysteine, ascorbic acid, uric acid, nitrate, and nitrite), at a H_2O_2 detection potential similar to the peroxidase enzyme. The ability of the biosensor system to perform routine analyses was demonstrated by the detection of H_2O_2 present in simulated milk and clinical and cosmetic samples with appreciable recovery values.

Keywords: biopolymers · carbon · electrochemistry · heme · nanotubes · sensors

Introduction

Trace impurities in carbon nanotubes (CNTs) such as graphitic carbon and metals of iron oxide, cobalt oxide, and nickel oxide were found to have unique electrochemical behaviors, especially electrocatalysis and electrochemical sensing. In 2006, Compton and co-workers first identified the electrocatalytic activity of a Fe impurity in the CNT for H_2O_2 reduction[1a,b] and hydrazine oxidation reactions.[1b,c] Later on, Pumera et al. reported the electrocatalytic activities of Fe_2O_3-[2a–d], NiO_3-,[2e,f] bimetallic Ni and Fe-,[2g] Co-, Mo-, and Fe[2h] impurities in multiwalled CNT (MWCNT), single-walled CNT (SWCNT), and double-walled CNT (DWCNT) towards some organic compounds such as organic peroxides,[2a] arginine, histidine,[2g] L-glutathione,[2e] sulfide[2f] and hydrazine,[2h] H_2O_2[2a,h] and glucose.[2c] Similarly, the presence of graphitic impurities within the CNT brings an electrocatalytic effect to hydroquinone,[3a] phenol,[3b] carbamazepine,[3c] azo groups,[3d] NADH,[3e] hydrazine,[3f] and biomolecule oxidation reactions.[3g] Recently, our group observed the improved molecular wiring of hemoglobin (Hb; heme protein) on the impure MWCNT.[4a] Although nanometallic impurities in the CNT are a unique source for derivatization, so far only a few reports are available for new CNT-impurity-based hybrid compounds.[4b,c] The availability of the impurities in a low concentration and difficulty in accessing the buried metallic sites inside the CNTs are limitations of the impurities for further derivatizations. Herein, we report the electro-assisted complexation of iron impurity in the MWCNT (MWCNT-Fe) with the amino functional group of chitosan (NH_2-CHIT) ([MWCNT-Fe:NH_2-CHIT]). The new hybrid chemically modified electrode showed a highly redox-active characteristic, which is similar to that of the redox and functional behaviors of heme peroxidase.

The design and development of an efficient heme enzyme biomimic is of considerable research interest in analytical, biochemical, and clinical chemistry due to the limitations of the features of the natural enzyme, which is found to have complicated isolation and purification steps, less stability, high cost, and easy denaturation.[5] In general, for any system to biomimic the natural enzyme, it would need to fulfill the following four key criteria: 1) structural and functional similarity, 2) matching of the redox potential, 3) op-

[a] P. Gayathri, Prof. A. S. Kumar
Environmental and Analytical Chemistry Division
School of Advanced Sciences
Vellore Institute of Technology University
Vellore-632 014 (India)
Fax: (+91) 416-2202754
E-mail: askumarchem@yahoo.com

Supporting information for this article is available on the WWW under http://dx.doi.org/10.1002/chem.201303075.

erational at a neutral pH conditions, and 4) high selectivity towards the target analyte. Considering the above criteria, the following representative compounds were reported as biomimics of heme peroxidase protein; porphyrins of Fe, Mn, and Co,[6a–d] hemin,[7a] and its functionalized compounds such as β-cyclodextrin-hemin,[7b] phytol-modified hemin[7c] and hemin carbon nanomaterial,[7d] ferric 2-hydroxy-1-naphthaldehyde thiosemicarbazone,[8a] Fe_3O_4 magnetic particles,[5,8b,c] hematin,[8d] prussian blue,[9a,b] Fe-*meso*-tetrakis[4-(*N*-trimethyl)aminophenyl]-porphophine, Fe-*meso*-tetrakis(4-*N*-methylpyridinium) porphophine,[9c] and FeS.[9d,e] Unfortunately, most of the existing compounds do not fulfill all the four biomimetic criteria. For instance, metal porphyrins and hemin have less selectivity because the compounds can also mediate other biochemicals such as nitrite, catechol, and dopamine.[10a–c] Prussian blue analogues shows less stability in neutral pH.[11a–d] Fe_3O_4 and FeS exhibit either zero or poor redox signatures.[5,9d,e] A new heme peroxidase biomimetic introduced in this work, [MWCNT-Fe:NH_2-CHIT], prepared by an electrochemical method on a glassy carbon electrode (GCE) showed highly selective, stable, efficient redox-active, and neutral pH-operational characteristics, unlike the conventional systems used for H_2O_2 reduction. The GCE/[MWCNT-Fe:NH_2-CHIT] is characterized by various physicochemical techniques such as field emission scanning electron microscopy (FESEM), transmission electron microscopy (TEM), Raman spectroscopy and Fourier transform infrared (FTIR) spectroscopic and electrochemical techniques (cyclic voltammetry (CV), rotating disc electrode (RDE), and amperometric *i–t* and flow injection analysis (FIA)). The analytical utility towards selective H_2O_2 sensing in various real samples (i.e., clinical, cosmetic, and milk) is also demonstrated in the final section of the work.

Results and discussion

Electrochemical characteristics of the biomimicking system: Figure 1 A displays 20 continuous CV responses of the [MWCNT + CHIT] mixer modified-GCE, (GCE/[MWCNT + CHIT]) scanned in a potential window −0.7 to +0.7 V versus Ag/AgCl at scan rate of 50 mV s^{-1} in pH 7 PBS (step 2, Scheme 1). A well-defined redox behavior (A1/C1) at an apparent standard electrode potential ($E^{\circ\prime} = E_{pa} + E_{pc}/2) = -(220 \pm 10)$ mV versus Ag/AgCl with surface excess (Γ) and relative standard deviation (RSD) values of 13.64 nmol cm^{-2} and 0.78 % (no. of cycles, $n = 10$), respectively, is deduced. The modified system, GCE/[MWCNT-Fe:NH_2-CHIT], is surface-confined electron-transfer in nature (the plot of the peak current vs. scan rate is linear, Figure 2 A and B) and follows the pH-dependent Nernstian characteristic (plot of E_{pc} vs. pH is linear and $\Delta E_{pc}/\Delta pH = -(30 \pm 3)$ mV, Figure 2 C and D). Control CV experiments of the single-material-modified systems, GCE/MWCNT and GCE/CHIT failed show any such interesting redox features (Figure 1 A, curves b and c). These observations showed a unique redox feature of the mixture chemically modified electrode (CMEs). Other forms of carbon, that is, functionalized (f-)MWCNT (Figure 1 B), purified (p-)MWCNT (Figure 1 C), graphite nanopowder (GNP, Figure 1 D) and activated carbon (AC, Figure 1 E) were also subjected to [Carbon + CHIT]-chemically modified electrode preparation such as in the case of GCE/[MWCNT-Fe:NH_2-CHIT] and CV studies were performed in pH 7 PBS. With the exception of the GCE/[f-MWCNT + CHIT] system, which showed $E^{\circ\prime}$ and Γ values of $-(110 \pm 5)$ V versus Ag/AgCl and 10.96 nmol cm^{-2}, respectively (Figure 1 B), none of the above CMEs displayed any marked redox signatures (Figure 1 C–E). Note that the $E^{\circ\prime}$ value obtained with [f-MWCNT + CHIT] (−110 mV vs. Ag/AgCl) is distinctly different from the value −220 mV vs. Ag/AgCl for the [MWCNT-Fe:NH_2-CHIT] system; however, it closely matches with the value −100 mV vs. Ag/AgCl for the previously reported f-MWCNT covalently grafted CHIT hybrid system (possibly through amide bonding, −C(=O)−NH−) -modified electrode prepared by chemical synthesis route).[12] From the above results, the following conclusions can be derived: 1) A specific and strong interaction between impure MWCNT with CHIT polymer; presumably, metal

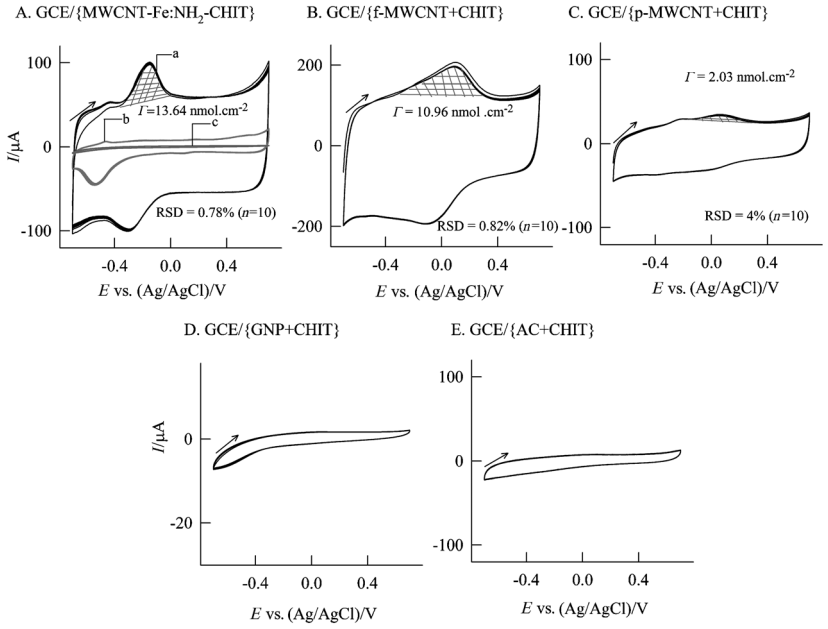

Figure 1. Continuous CV responses of A) GCE/[MWCNT-Fe:NH_2-CHIT] (curve a), GCE/MWCNT (curve b) and GCE/CHIT (curve c), B) GCE/[f-MWCNT + CHIT], C) GCE/[p-MWCNT + CHIT], D) GCE/[GNP + CHIT], and (E) GCE/[AC + CHIT] in pH 7 PBS at a scan rate 50 mV s^{-1}.

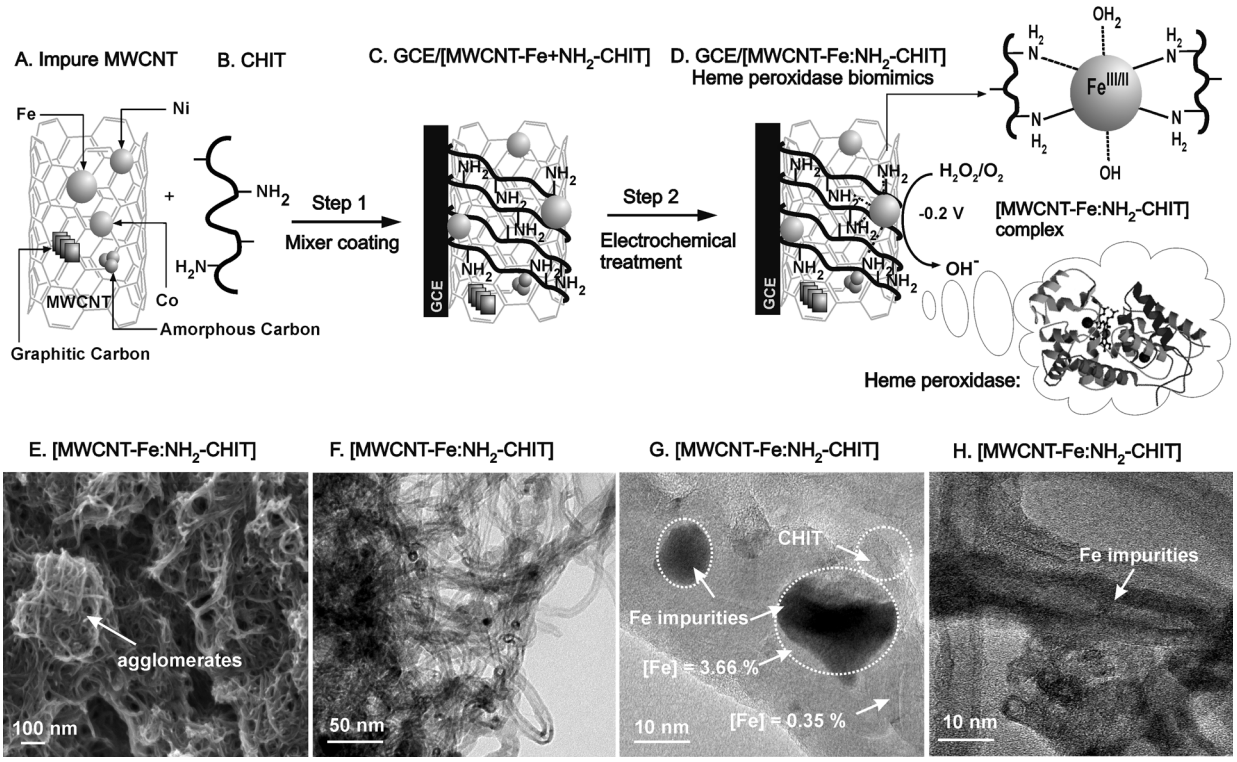

Scheme 1. A)–D) Schematic illustration for the fabrication of GCE/[MWCNT-Fe:NH_2-CHIT] and E) SEM and F)–H) TEM images.

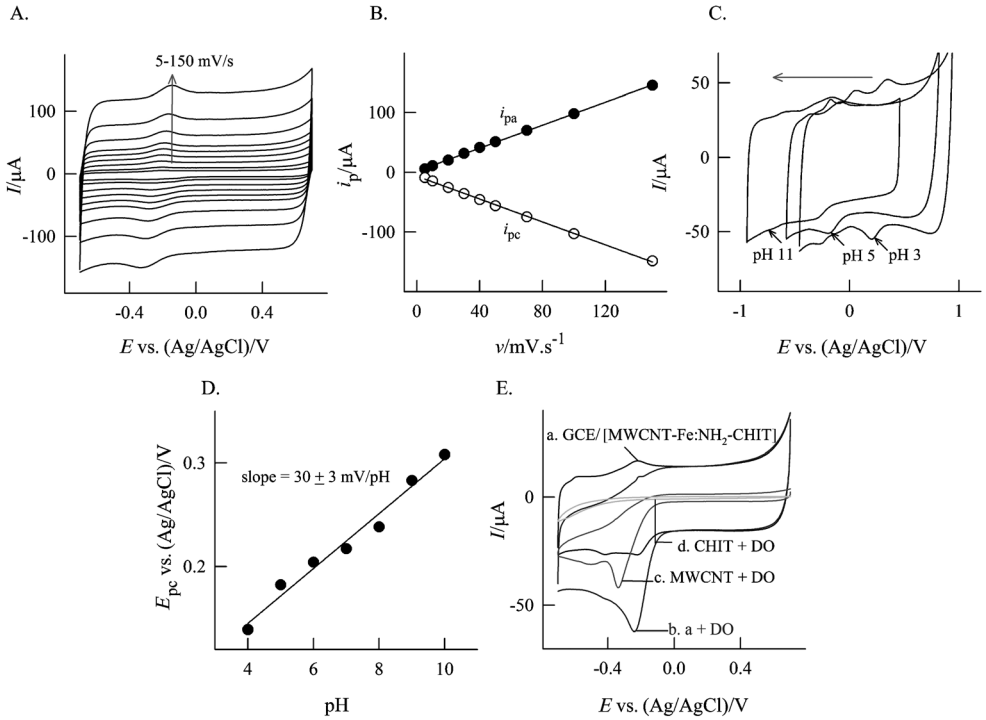

Figure 2. A) Effect of scan rate on CV response of GCE/[MWCNT-Fe:NH_2-CHIT] in pH 7 PBS; B) plot of peak currents versus scan rate; C) effect of solution pH on CV response of GCE/[MWCNT-Fe:NH_2-CHIT] at scan rate = 50 mV s^{-1}; D) plot of E_{pc} versus pH, and E) CV responses of GCE/[MWCNT-Fe:NH_2-CHIT] without (curve a) and with saturated dissolved oxygen (DO; curve b), GCE/MWCNT (curve c), and GCE/CHIT (curve d) with saturated DO in pH 7 PBS at a scan rate of 10 mV s^{-1}.

impurities in the MWCNT and the amino functional group of CHIT may form a coordination complex and 2) the redox potential of the GCE/[MWCNT-Fe:NH_2-CHIT] is comparable to the standard E^o value of the heme peroxidase system ($-(270\pm10)$ mV vs. the saturated calomel electrode or $-(225\pm10)$ mV vs. Ag/AgCl).[13a,b]

To obtain precise structural details, the [MWCNT-Fe:NH_2-CHIT] system was subjected to several physicochemical characterizations and the results are summarized below:

1) SEM images of pristine-MWCNT and the hybrid displayed in the Figure S1 A and B (the Supporting Information) and Scheme 1 E showed white-colored polymeric objects wrapped around the surface of MWCNT, possibly the CHIT on the CNT.
2) TEM characterization of the hybrid provides supportive information about the impurities as smaller black-colored particles and CHIT layer as a dark-grey-colored continuous layer wrapped around the CNT (Scheme 1 F–H and Figure S1 C, the Supporting Information). The iron content in the hybrid system on the black-colored selective spot area calculated by using EDAX was 3.66 % (36 600 ppm). The value at other CNT walls area was 0.35 % (3500 ppm). Raman spectrum response (Figure 3 A) of an optimal screen-printed electrode (SPE)-Au/[MWCNT-Fe:NH_2-CHIT] (step II conditioned; the optimal; curve c) ($I_D/I_G=0.41$) in comparison with several control systems, SPE-Au/[MWCNT+CHIT] (step I conditioned, i.e., before the electrochemical cycling; curve b) ($I_D/I_G=0.56$) and SPE-Au/MWCNT (curve a) ($I_D/I_G=0.62$) yielded a significant decrement in the ratio (I_D/I_G) of D (disorder graphitic structure) and G (graphitic structure) band peaks. The decreased ratio value may indicate a specific interaction of MWCNT with CHIT.[14] Since the impure MWCNT-coupled CHIT showed effective redox behavior, we expect the impurities present in the MWCNT might have a specific role for the interaction. It has been reported that metal oxides, such as Fe_2O_3, Co_3O_4, NiO, and carbonaceous species like graphite and amorphous carbon are present in trace amounts within the MWCNT as impurities.[2a,3a,4a] To find out which metal impurity is responsible for the interaction with CHIT, the metal oxides; Fe_2O_3, Co_3O_4, and NiO were discreetly combined with CHIT for chemically modified glassy carbon electrode preparation as in the optimal electrode ([MWCNT-Fe:NH_2-CHIT]) and then subjected to CV and H_2O_2 electrocatalytic studies. It was expected that electrocatalysis of the metal complex would be much better than in the metal oxide systems. As can be seen in Figure S2 (the Supporting Information), the [Fe_2O_3+CHIT] composite yielded a very feeble redox feature at $E^{\circ\prime}=-(480\pm5)$ mV versus Ag/AgCl and showed an eight times higher H_2O_2 reduction reaction signal than the Fe_2O_3, NiO, Co_3O_4, [NiO+CHIT], and [Co_3O_4+CHIT] composite systems. Note

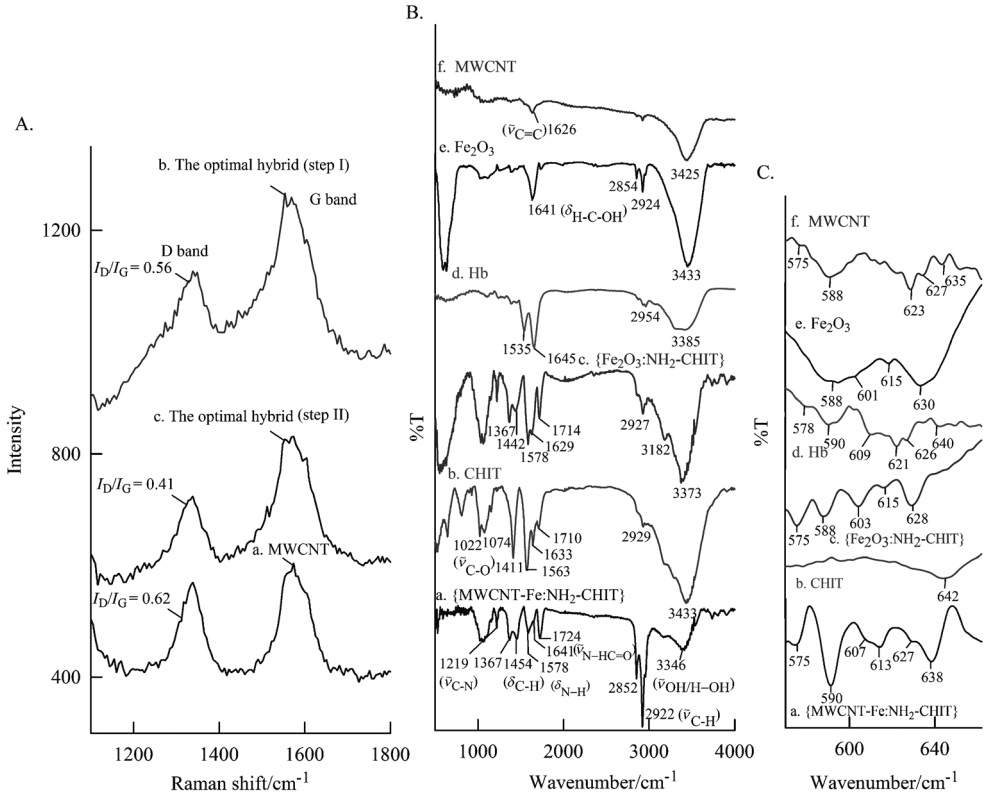

Figure 3. A) Raman spectroscopy and B) and C) FTIR/KBr responses of [MWCNT-Fe:NH_2-CHIT] and its control systems.

that with the exception of [Fe_2O_3+CHIT] (Figure S2 A, the Supporting Information), none of the other control systems including [NiO+CHIT], (Figure S2 B) and [Co_2O_3+CHIT] (Figure S2 C) failed to show any significant redox feature in this study. This observation speculates specific role of iron oxide within the MWCNT for further interaction with CHIT. In fact, a four- or six-coordinated Fe^{III}-Chitosan complex has already been reported in the literature.[15a,b] Because the environment structure of impure Fe and bulk Fe_2O_3 are different, there was difference in the $E^{\circ\prime}$ of the respective hybrids. It is expected that during the electrochemical pre-treatment step (Scheme 1, step 2), the iron impurity existing in the form of Fe metal or Fe_2O_3 might be electrochemically converted to an iron ion (Fe^{2+} and Fe^{3+}) and subsequently involved in the complexation. Note that analysis of the trace metal by using electrothermal atomic absorption spectrometry (ETAAS) showed the Fe content values 21000 (2.1%), 6000 (0.6%) and 6000 ppm (0.6%), respectively, with the bulk pristine-, functionalized- and purified-MWCNT samples. Observation of selective redox behavior with the pristine MWCNT+CHIT system (Figure 1 A) may indicate the inaccessibility of the Fe in the p-MWCNT and f-MWCNT by the CHIT polymer. On the other hand, an Fe content of 21000 ppm may be the optimal value for efficient [MWCNT-Fe:NH_2-CHIT] complexation.

3) The FTIR response of [MWCNT-Fe:NH_2-CHIT] displayed in Figure 3 B further supports the above observations. As can be seen with the optimal system (curve a) specific peaks correspond to amino group at 1578 cm^{-1} ($\delta_{N\text{-}H}$) and carbonyl group (>C=O) from the amide site of CHIT at 1641 cm^{-1} ($\nu_{N\text{-}HC=O}$). A control FTIR of CHIT (curve b) yielded similar-fashioned peaks but with 15 (1563 cm^{-1}) and 8 cm^{-1} (1633 cm^{-1}) shifts in the corresponding values, which might be due to the coordination complex interaction. An extended control experiment with a [Fe_2O_3+CHIT] chemically modified electrode (curve c) (prepared as in the optimal case) displayed an identical amino function group value to that of the [MWCNT-Fe:NH_2-CHIT] (1578 cm^{-1}). For comparison, the FTIR response of a heme protein (Hb) is also displayed in Figure 3 B (curve d), in which the amide I (1645 cm^{-1}) and amide II (1535 cm^{-1}) peaks resemble the amide functional group of [MWCNT-Fe:NH_2-CHIT]. Similarly, at a low frequency region (570–660 cm^{-1}; Figure 3 C), the values due to the Fe–O/Fe–N stretching of heme (578, 590, 609, 621, 626 and 640 cm^{-1}) closely match the values for the [MWCNT-Fe:NH_2-CHIT] (575, 590, 607, 613, 627, and 638 cm^{-1}) and [Fe_2O_3-CHIT] (575, 588, 603, 615, and 628 cm^{-1}) systems. No such unique behavior was observed with individual samples; CHIT, MWCNT, and Fe_2O_3. Based on the pH-dependent electrochemical behavior (Figure 2 C and D), Fe_2O_3-based control experiment (Figure S2, the Supporting Information), and physicochemical characterization data (Figure 3 and Scheme 1 E–H), a possible structure for [MWCNT-Fe:NH_2-CHIT] is sketched in Scheme 1 D; in which the Fe of the MWCNT is complexed with CHIT-NH_2 and hydroxy/H-OH ligands (FTIR, $\nu_{OH/H\text{-}OH}$ $\approx$3350 cm^{-1}) in a six-coordinated $Fe^{III/II}$ arrangement similar to the heme peroxidase active site.

To understand the intriguing mechanistic feature and biomimetic functional activities of the hybrid [MWCNT-Fe:NH_2-CHIT] system, several more control experiments and hydrogen peroxide electrochemical reduction tests were also performed. Figure 4 A–E are typical CV responses of various hybrid [carbon-CHIT] chemically modified GCEs for H_2O_2 electrochemical activity in pH 7 PBS at ν= 10 mV s^{-1}. The GCE/[MWCNT-Fe:H_2N-CHIT] showed a H_2O_2 reduction peak potential (E_{cat}) at −0.16 V versus Ag/AgCl, in which the A1/C1 redox peak exists (Figure 4 A, curves a and b); whereas the unmodified GCE/MWCNT displayed about a 200 mV increased overpotential and $\approx$50% decreased peak current values when compared with the optimal case (Figure 4 A, curve c). The H_2O_2 reduction on the optimal electrode is diffusion-controlled electron-transfer in nature (data not enclosed) and showed a CV calibration plot in the concentration window of 100–2500 μM with a current sensitivity value of 80 nA μM^{-1} (inset plot Figure 5 A). Other forms of CNT chemically modified electrodes, that is, GCE/[f-MWCNT+CHIT] (Figure 4 B) and GCE/[p-MWCNT+CHIT], (Figure 4 C) yielded overpotentials of about 300 and 400 mV, respectively, when compared with the optimal case for the H_2O_2 reduction. Extended experiments with bulk carbon materials, GCE/[GNP+CHIT] (Figure 4 D) and GCE/[AC+CHIT] (Figure 4 E) also resulted in poor H_2O_2 reduction current signals. Hence, it is clear that the [MWCNT-Fe:NH_2-CHIT] hybrid system has superior electrochemical performance and functional similarity with the heme peroxidase.

The electrocatalytic function of the biomimetic system was further analyzed by using the RDE technique, in which a RDE-glassy carbon electrode was modified with [MWCNT-Fe:NH_2-CHIT] and subjected to CV at slow scan rate (10 mV s^{-1}) under various hydrodynamic rotation speeds (50–1000 rpm) as in Figure 6 A. Systematic increases in the current response against increase in the rpm values were noticed. The system follows the Levich Equation: $i_{L,E}=[0.62nFAD^{2/3}\nu^{-1/6}C_o^*]\omega^{1/2}$, in which a linear response of hydrodynamic current, measured at different potentials (E); −0.4 (E_1), −0.45, −0.5, −0.55, −0.6, −0.65, −0.7, and −0.75 V versus Ag/AgCl (E_8) against the square route of angular velocities, was noticed (Figure 6 B). The following Koutecky–Levich Equations (1)and (2) were applied for the kinetic parameter calculation:[16a,b]

$$1/i_{L,E} = 1/i_k + 1/0.62nFAD^{2/3}\nu^{-1/6}\omega^{-1/2}C_o^* \quad (1)$$

$$i_k = nFAk_hC_o^*\Gamma \quad (2)$$

in which k_h is the heterogeneous rate constant of the H_2O_2 reduction reaction on the biomimetic system-modified elec-

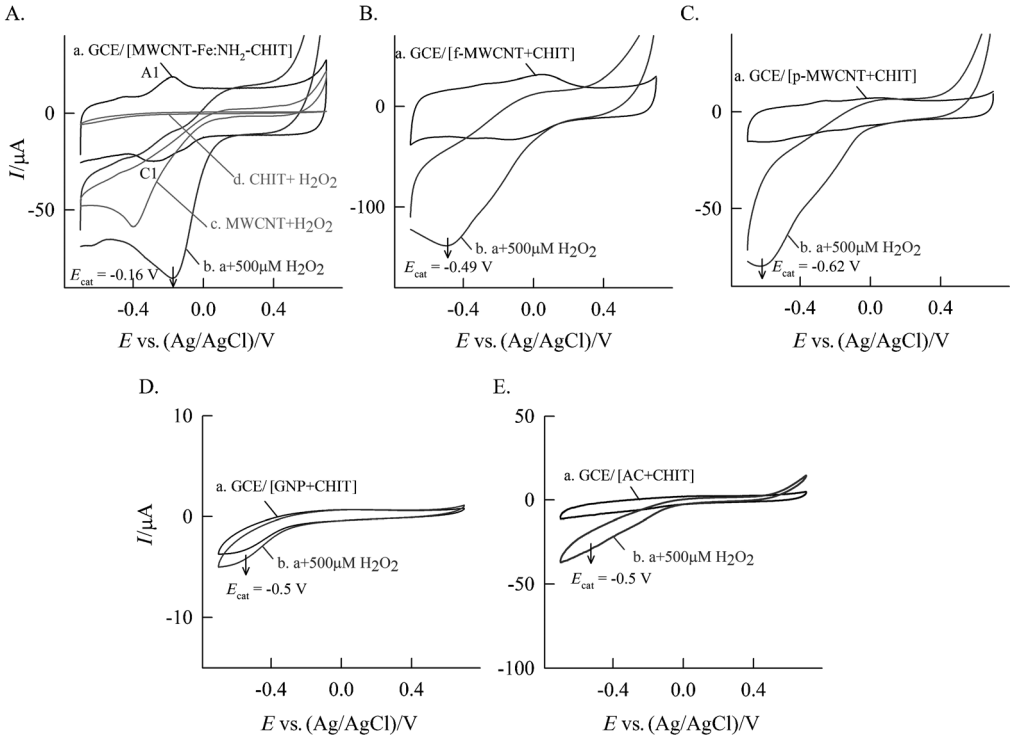

Figure 4. CV responses of A) GCE/{MWCNT-Fe:NH_2-CHIT} (curve b), GCE/MWCNT (curve c), and GCE/CHIT with 500 μM of H_2O_2 (curve d), and curve a is the GCE/[MWCNT-Fe:NH_2-CHIT] response without the analyte; B) GCE/[f-MWCNT + CHIT], C) GCE/[p-MWCNT + CHIT], D) GCE/[GNP + CHIT], and E) GCE/[AC + CHIT] without (curve a) and with 500 μM of H_2O_2 (curve b) in pH 7 PBS at $v = 10\,mV\,s^{-1}$. E_{cat} = Electrocatalytic potential.

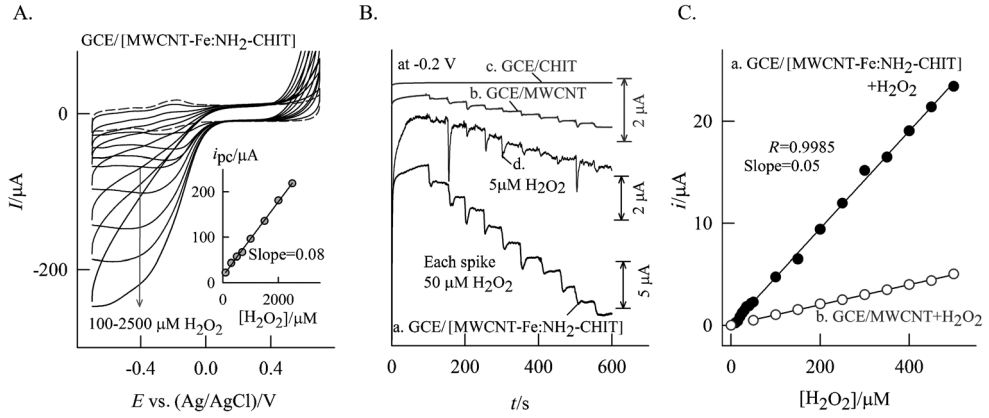

Figure 5. A) Effect of H_2O_2 concentration on the CV response of GCE/[MWCNT-Fe:NH_2-CHIT] in pH 7 PBS at $v = 10\,mV\,s^{-1}$. Inset plot is $[H_2O_2]$ versus i_{pc}; B) Amperometric *i*–*t* response of GCE/[MWCNT-Fe:NH_2-CHIT] (curves a and d), GCE/MWCNT (curve b), GCE/CHIT (curve c) with 5 (curve d), or 50 μM H_2O_2 spikes at an applied potential of −0.2 V versus Ag/AgCl in pH 7 PBS and C) calibration plot of $[H_2O_2]$ versus current.

trode surface, i_k is the kinetic current, $i_{L,E}$ is the current measured at limiting current (L) or different potentials (E), ω is the angular velocity, C_o* is the H_2O_2 analyte concentration, F is the Faraday constant, A is the electrode area (cm^2), and D is the diffusion coefficient. A plot of $i_{L,E}^{-1}$ versus $\omega^{-1/2}$ yielded linear lines and the respective i_k values were calculated from the intercepts (Figure 6C). Finally, the value of $k_h = 1.11 \times 10^9\,mol^{-1}\,cm^3\,s^{-1}$ can be obtained by applying the i_k values into Equation (2). Note that this value is comparable to the metal–porphyrin-based biomimetic system for the H_2O_2 electrocatalysis ($1.2 \times 10^9\,mol^{-1}\,cm^3\,s^{-1}$).[6d]

To provide evidence to further support the biomimic function of the new system, we also subjected the electrode to the dissolved oxygen (DO) reduction reaction, as in the heme function,[17] shown in Figure 2E. It is interesting to notice that the [MWCNT-Fe:NH_2-CHIT] system showed excellent electrocatalytic DO reduction, which enhanced the current signal by about two-fold and resulted in about

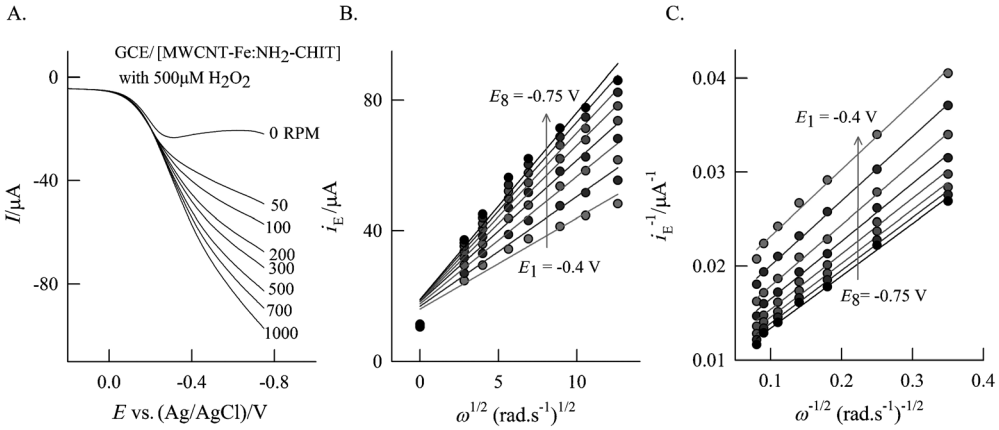

Figure 6. (A) RDE responses for the reduction of 500 μM H_2O_2 on GCE/[MWCNT-Fe:NH_2-CHIT] at different rotation speeds (50–1000 rotations per minute (rpm)) at $v = 10\,mV\,s^{-1}$; (B) Levich and (C) Koutecky–Levich plots at different potentials (E_1–E_8: −0.4, −0.45, −0.5, −0.55, −0.6, −0.65, −0.7, and −0.75 V versus Ag/AgCl) for the RDE response.

a 200 mV reduction in the overpotential compared with the unmodified electrode (GCE/MWCNT). Table 1 summarizes some of the structural and functional similarities of MWCNT-CHIT relative to the heme protein (hemoglobin). Overall, it is obvious that the new system introduced in this work is unique for biomimetic function. The electroanalytical application of the biomimetic system is further demonstrated in next section.

Table 1. Comparison of some of physical and functional parameters of GCE/[MWCNT-Fe:NH_2-CHIT] with the heme protein.

No.	GCE/[MWCNT-Fe:NH_2-CHIT]	Heme protein
S1	$Fe^{III/II}$ redox system	$Fe^{III/II}$ redox system
S2	Characteristic IR peaks: 1641 cm^{-1} (amide I band), 1578 cm^{-1} (amide II band) and 590 cm^{-1} (Fe–O vibration)	Characteristic IR peak: 1645 cm^{-1} (amide I band), 1535 cm^{-1} (amide II band) and 590 cm^{-1} (Fe–O vibration)
S3	$E° = -(220\pm10)$ mV vs. Ag/AgCl	$E° = -(380\pm10)$ mV vs. Ag/AgCl
S4	O_2 catalysis	O_2 catalysis
S5	H_2O_2 electrocatalysis at −0.16 V vs. Ag/AgCl (starting potential)	H_2O_2 electrocatalysis at −0.12 V vs. Ag/AgCl (starting potential)
S6	Other chemicals: No interference	Other chemicals: No interference

Analytical application: The GCE/[MWCNT-Fe:NH_2-CHIT] showed excellent amperometric *i–t* sensing response to H_2O_2 in physiological solution. As can be seen in Figure 5B, spikes of 50 μM of H_2O_2 at the applied potential of −0.2 V versus Ag/AgCl showed systematic increase in the current signals (curve a); whereas the unmodified electrodes such as GCE/MWCNT (curve b) and GCE/CHIT (curve c) failed to show any such current responses. A plot of the amperometric current against the concentration of H_2O_2 (Figure 5C) shows that [H_2O_2] is linear up to 400 μM, with current sensitivity and regression coefficient values of $50\,nA\,\mu M^{-1}$ ($0.7072\,A M^{-1} cm^{-2}$) and 0.9985, respectively. Ten successive spikes of 5 μM of H_2O_2 resulted in a relative standard deviation (RSD) value of 2.6% (Figure 5B, curve d). The calculated detection limit (signal-to-noise ratio = 3) is 2.3 μM. The sensitivity and detection limit values obtained were relatively better than that of other biomimicking and enzyme systems such as hemin–carbon nanofiber ($0.002\,A M^{-1} cm^{-2}$ and 2 μM) and hemin–carbon nanotube ($0.024\,A M^{-1} cm^{-2}$ and 30 μM),[7d] FeS nanoparticles/glutaraldehyde ($0.026\,A M^{-1} cm^{-2}$ and 4.03 μM)[9e] and HRP immobilized sol–gel ceramic CNT ($0.0057\,A M^{-1} cm^{-2}$ and 12.89 μM)[17] chemically modified electrodes. Most importantly, in contrast to the previous cases with serious interference, the [MWCNT-Fe:NH_2-CHIT] showed a tolerable current signal to other biochemicals such as NO_2^- (hemin- and Fe_3O_4-modified electrodes),[7d,8b] ascorbic acid (hemin- and iron-(III) porphyrin-modified electrodes),[7a,6b] cysteine (Fe_3O_4-graphene oxide[8c] and Prussian blue[9b] systems) and uric acid (Figure S3, the Supporting Information).[7a,6b]

The amperometric *i–t* response was further extended to allow the calculation of some kinetic parameters by the Michaelis–Menten (MM) mechanism. A possible reaction pathway for the reduction of H_2O_2 by the biomimetic system is given in the Scheme 2, in which the analyte H_2O_2 first binds on the reduced form of the biomimetic site reversibly (step 1), followed by the reduction of the H_2O_2 with the simultaneous formation of oxidized form of the biomimic,

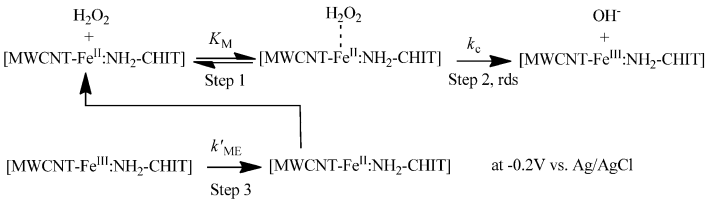

Scheme 2. Michaelis–Menten reaction pathway for the electrocatalytic reduction of H_2O_2 on GCE/[MWCNT-Fe:NH_2-CHIT]; rds = rate-determining step.

that is, [MWCNT-Fe^{III}:NH_2-CHIT] through an inner-sphere electron-transfer mechanism (step 2). Finally, the active site, [MWCNT-Fe^{II}:NH_2-CHIT] is regenerated at the A1/C1 operating potential as in step 3. K_M, the apparent MM constant (mM), k_c, the first order chemical rate constant (s^{-1}) and k'_{ME}, the heterogeneous modified-electrode rate constant ($cm\,s^{-1}$) were deduced from the following MM Equation by using the Lineweaver–Burk approach as per our previous reported procedure[18a–c] for the catalytic current; the values are $k_c = 0.28\,s^{-1}$, $K_M = 0.23$ mM and $k'_{ME} = 16\times10^{-3}\,cm\,s^{-1}$. Note that the K_M value obtained in this work is less than the reported literature K_M values of 1.27 mM (FeS nanoparticles biomimicking peroxidase system),[9e] 0.66 mM (Nf-HRP/PS-MWCNT/Au)[19a] and 1.35 mM (HRP/CNT-Sol–gel).[19b] This observation represents the higher catalytic activity of the present system.[4a]

In addition, the FIA of H_2O_2 was also studied by using a FIA-GCE/[MWCNT-Fe:NH_2-CHIT] as a electrochemical detector. Interrelated hydrodynamic parameters were optimized individually at a flow rate of $0.75\,mL\,min^{-1}$ and applied potential (E_{app}) of −0.2 V versus Ag/AgCl. A reproducible current–time response was obtained upon successive injections of different H_2O_2 concentrations range from 100 to 500 μM (Figure 7A, curve a). Meanwhile, as a control experiment, a sol–gel polymeric system that does not have amino terminal to complex with iron system was also combined with MWCNT. It was prepared as in the case of the biomimetic electrode, designated as the GCE/[MWCNT-sol–gel], and also subjected to FIA of H_2O_2. As expected, the above sol–gel-modified system failed to show any H_2O_2 signal (Figure 7A, curve b), which may be due to the absence of the unique complex formation. The biomimetic detector showed a calibration plot in the H_2O_2 concentration window of 50 to 2500 μM with a sensitivity value of $0.59\,nA\,\mu M^{-1}$ ($0.8345\,A\,M^{-1}\,cm^{-2}$; Figure S4, the Supporting Information). This value is comparable to the value of $0.56\,nA\,\mu M^{-1}$ with the MWCNTs-HRP enzyme-based flow injection analysis with electrochemical detection (FIA-ECD) system.[20] Ten continuous spikes of 50 μM of H_2O_2 yielded an RSD of 5%. The calculated detection limit (signal-to-noise ratio = 3) value by the FIA method is 9.7 μM. The FIA-ECD was also subjected to detection of various biochemicals; cysteine (CysH), ascorbic acid (AA), uric acid (UA), nitrate (NO_3^-), and nitrite (NO_2^-). As in the amperometric *i*--*t* response in Figure S3 (the Supporting Information), no interference was noticed in the FIA (Figure 7B). This observation implies a highly selective detection of H_2O_2 in this work, similar to enzyme-based detection methodologies. Finally, to validate the biomimetic-based detection approach, three real H_2O_2-containing samples: a clinical (sample 1) (Figure 7C), a cosmetic (sample 2), and a milk sample (sample 3; see the Experimental Section (procedures) for further details), were subjected FIA-ECD by using a standard addition approach method.[21] Table S1 (the Supporting Information), shows the detailed information of H_2O_2 detection. The original detected values of clinical and cosmetic samples are 88.75 and 1.25 μM, respectively. The calculated recovery values were ≈100%, which indicates the appreciable analytical performance of the system.

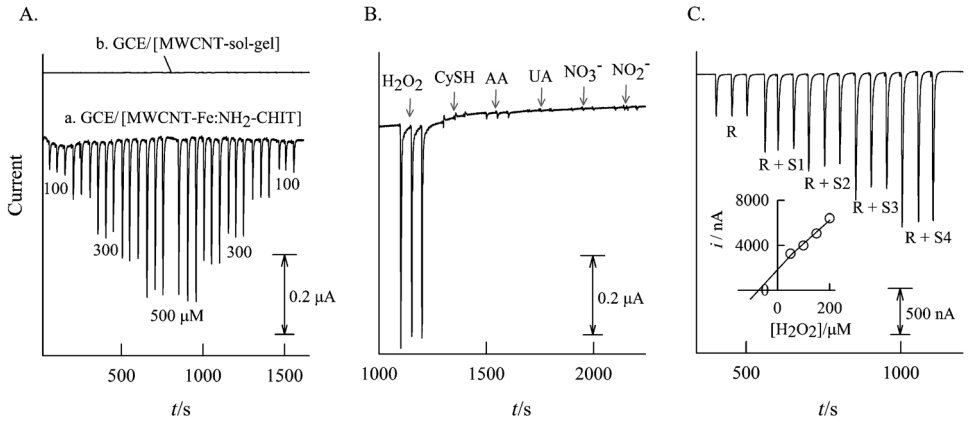

Figure 7. A) FIA responses of a) GCE/[MWCNT-Fe:NH_2-CHIT] and b) GCE/[MWCNT-sol–gel] with different [H_2O_2]; B) Effect of interference of various biochemicals at H_2O_2 sensing conditions; C) Real sample analysis for the detection of H_2O_2 in clinical sample at a fixed potential, $E_{app} = -0.2$ V versus Ag/AgCl and flow rate, $H_f = 0.75\,mL\,min^{-1}$ in pH 7 PBS.

Conclusion

An impure multiwalled carbon nanotube–chitosan polymer hybrid composite chemically modified glassy carbon electrode, GCE/[MWCNT-Fe:NH_2-CHIT] was prepared and a unique electrochemical redox behavior at $E^{\circ\prime} = -0.22$ V versus Ag/AgCl in pH 7 PBS was observed. The redox system mediates hydrogen peroxide and dissolved oxygen reduction reactions in neutral pH solution. Control experiments with purified- and functionalized-MWCNT combined chitosan polymer systems failed to show any such unique electrochemical/electrocatalytic features. The new composite system was characterized by using FESEM, TEM, Raman spectroscopy, FTIR, and electrochemical techniques. Several control experiments using iron oxide, cobalt oxide, nickel oxide, graphite, and activated carbon combined with chitosan were tested for the electrochemical activity. It has been revealed that combining the iron impurity in the MWCNT complexes with the amino functional group of chitosan can yield the unique electrochemical and electrocatalytic features in neutral pH, similar to the heme peroxidase function. A mechanism for the electrocatalytic function of H_2O_2 was explained in terms of Mi-

chaelis–Menten-type enzymatic kinetics, in which the reduced form of the iron(II)-chitosan complex mediated the reduction reaction. The calculated heterogeneous rate constant value, k_h, obtained by the rotating disc electrode technique, was matched with the porphyrin-based biomimetic system data. Analytical application of the new peroxidase biomimic for H_2O_2 sensing was demonstrated by using amperometric *i–t* and flow injection analysis methods. In contrast to previous literature reports, which showed serious interference with co-existing biochemicals or instability in neutral pH solution, the system showed negligible interference of other co-existing biochemicals, such as cysteine, nitrite, nitrate, uric acid, and ascorbic acid, as in the peroxidase enzyme function. Finally, applications of the present biomimetic system to test the H_2O_2 in various real samples were successfully demonstrated with ≈100% recovery values. Overall, the present work is unique in following respects: 1) a specific report for the derivatization of iron impurity in MWCNT with chitosan to a new coordination complex system, 2) the first report for the biomimetic function of the iron impurity in MWCNT, 3) the present hybrid electrode fulfills all the necessary criteria of a biomimetic system and 4) it is extendable to the analysis of several real samples.

Experimental Section

Chemicals and reagents: MWCNT, (>90% carbon basis, outer diameter: 10–15 nm; inner diameter: 2–6 nm; length 0.1–10 μm), nickel(II) oxide nanopowder of size 50 nm (99.8% trace metal basis) and iron(II,III) oxide nanopowder of size 50 nm (≈98% trace metal basis) were obtained from Sigma–Aldrich. Cobalt oxide (99% purity) was obtained from SRL, India. Graphite nanopowder (GNP; 400 nm, ≈98% purity) was purchased from SRL, India. Hydrogen peroxide was obtained from Rankem, India and stored in a refrigerator. Other chemicals used were all of analytical grade and used without further purification. Screen-printed gold (SPE-Au) and -carbon electrodes (SPCE) (0.0707 cm^2) were gifted by Prof. Jyh-Myng Zen. Aqueous solutions were prepared using deionized and alkaline potassium permanganate distilled water (designated as DD water). The supporting electrolyte, pH 7 phosphate buffer solution (PBS) of ionic strength $I = 0.1\ mol\,L^{-1}$ was used throughout this work.

Instrumentation: Voltammetric measurements were carried out with CHI models 440B (for CV) and 760D (for RDE) electrochemical workstation (USA). The three-electrode system consisted of a glassy carbon (Tokai, Japan, 3 mm diameter, 0.0707 cm^2 area), or of a chemically modified form, as the working electrode, Ag/AgCl as the reference electrode, and a platinum wire as the auxiliary electrode. Glassy carbon Rotating disk electrode (0.0707 cm^2) was purchased from Bioanalytical systems Inc (BAS), USA (Model- RRDE-3A). The FIA system consisted of Hitachi L-2130 pump delivery (Japan), a Rehodyne model 7125 sample injection valve (20 μL loop) with interconnecting Teflon tube and a conventional electrochemical detector system (BAS, USA). High-resolution TEM with Energy dispersive X-ray analysis (EDAX) measurements were performed by using a JEOL JEM 2100 instrument (Japan). A Zeiss SMT, Ultra plus (Germany) instrument along with Oxford X-ray probe was used for field emission scanning electron microscope (FESEM) studies. For the FTIR analysis, a JASCO 4100 Spectrophotometer (Japan) was used with the KBr method. Raman spectroscopy analysis was carried out using AZILTRON, PRO 532 (USA) with a 532 nm laser excitation source. X-ray photoelectron spectroscopy was performed using Ulvac-PHI, PHI500, Versaprobe instrument (USA). Trace metal impurity measurements were performed by using a continuum source electrothermal atomic absorption spectrometry instrument (ZEEnit 65 model, Analytika Jena AG, Jena, Germany).

Procedures: Purified- and functionalized-MWCNT (i.e., p-MWCNT and f-MWCNT, respectively) were prepared by heating pristine MWCNTs (200 mg) in 35 mL of 6 M (for p-MWCNT) or 15 M HNO_3(for f-MWCNT) in a silicone oil bath at reflux for 12 h ($T = 413(\pm 2)$ K/140 °C). The product was filtered and washed with copious amount of DD H_2O until the pH of the filtrate solution become neutral and the samples were dried at $T = (350 \pm 5)$ K (80 °C) in a vacuum oven.[4a] Physicochemical characterization of pristine MWCNT by using TGA and XRD showed presence of impurities (6.88%), which is due to metal oxides such as iron oxide, nickel oxide, cobalt oxide, and other carbon materials (graphitic carbon and amorphous carbon). CS-ETAAS analysis showed the following contents of trace impurities with the CNTs: MWCNT (Fe 21000 ppm; Ni 14 ppm; Co 1.6 ppm), f-MWCNT (Fe 6000 ppm; Ni 11 ppm; Co 1.6 ppm) and p-MWCNT (Fe 6000 ppm; Ni 29 ppm; Co 7 ppm).

A stock solution of CHIT (0.5 wt%) was prepared by mixing CHIT flakes (50 mg) with 1% glacial acetic acid (10 mL), stirred for 3 h at RT until complete dissolution, and the pH was adjusted to 4–5 using a concentrated NaOH solution. Similarly, a stock dispersion of [CHIT+MWCNT] was prepared by sonicating a mixture of MWCNT (1 mg) and the 0.5 wt% CHIT (500 μL) for (15±1) min. Then, the chemically modified biomimicking electrode, GCE/[MWCNT-Fe:NH_2-CHIT] was fabricated by using a two-step procedure. In the first step, an aliquot of the [CHIT+MWCNT] stock solution (10 μL) was drop-casted on a cleaned GCE (designated as GCE/[MWCNT+CHIT]) and dried in air for (15±3) min at RT (step 1, Scheme 1) and then electrochemically conditioned at a potential window of −0.7 to 0.7 V versus Ag/AgCl at a scan rate of 50 $mV\,s^{-1}$ in pH 7 PBS for 20 continuous CV cycles (step 2, Scheme 1). All other control chemically modified electrodes (CMEs) were prepared in a way similar to the above case with 1 mg/500 μL CHIT solution of various carbons and metal oxide materials. For the FTIR and TEM analyses, the as-prepared SPE-Au/[MWCNT-Fe:NH_2-CHIT] film (dried in a desiccator for overnight) was carefully peeled off from the surface using a doctor's needle (0.5 mm×3.5 cm) and subjected to further examinations. SEM and Raman spectra characterizations were performed using SPE-Au/[MWCNT-Fe:NH_2-CHIT]-modified electrodes. The H_2O_2-containing samples (sample 1: a clinical hydrogen peroxide solution (no detail for the H_2O_2 concentration) obtained from the VIT university healthcare center; sample 2: a cosmetic fairness bleach cream (Fem, India), purchased from a local departmental store, and sample 3: a pasteurized milk sample (aavin milk) obtained from local milk shop) were subjected to real sample analyses. There were no displays about the H_2O_2 content in the labels of the real samples.

Acknowledgements

The authors are grateful to the Department of Science and Technology-Science and Engineering Research Council Scheme (DST-SERC) for the financial support. We also thank DST-Technology System Development for the FIA-ECD.

[1] a) B. Sljukic, C. E. Banks, R. G. Compton, *Nano Lett.* **2006**, *6*, 1556–1558; b) J. Kruusma, N. Mould, K. Jurkschat, A. Crossley, C. E. Banks, *Electrochem. Commun.* **2007**, *9*, 2330–2333; c) C. E. Banks, A. Crossley, C. Salter, S. J. Wilkins, R. G. Compton, *Angew. Chem.* **2006**, *118*, 2595–2599; *Angew. Chem. Int. Ed.* **2006**, *45*, 2533–2537.

[2] a) E. J. E. Stuart, M. Pumera, *J. Phys. Chem. C* **2010**, *114*, 21296–21298; b) M. Pumera, Y. Miyahara, *Nanoscale* **2009**, *1*, 260–265; c) L. Siegert, D. K. Kampouris, J. Kruusma, V. Sammelselg, C. E. Banks, *Electroanalysis* **2009**, *21*, 48–51; d) M. Pumera, A. Ambrosi, E. L. K. Chng, *Chem. Sci.* **2012**, *3*, 3347–3355; e) A. Ambrosi, M. Pumera, *Chem. Eur. J.* **2010**, *16*, 1786–1792; f) E. L. K. Chng, M. Pumera, *Chem. Asian J.* **2011**, *6*, 2304–2307; g) M. Pumera, H. Iwai,

Y. Miyahara, *ChemPhysChem* **2009**, *10*, 1770–1773; h) M. Pumera, H. Iwai, *J. Phys. Chem. C* **2009**, *113*, 4401–4405.
[3] a) E. J. E. Stuart, M. Pumera, *Chem. Asian J.* **2011**, *6*, 1019–1021; b) E. J. E. Stuart, M. Pumera, *J. Phys. Chem. C* **2011**, *115*, 5530–5534; c) E. L. K. Chng, M. Pumera, *Electrochem. Commun.* **2011**, *13*, 781–784; d) E. J. E. Stuart, M. Pumera, *Chem. Asian J.* **2011**, *6*, 804–807; e) E. J. E. Stuart, M. Pumera, *Chem. Eur. J.* **2011**, *17*, 5544–5548; f) E. J. E. Stuart, M. Pumera, *Phys. Chem. Chem. Phys.* **2011**, *13*, 10818–10822; g) E. L. K. Chng, M. Pumera, *Chem. Eur. J.* **2012**, *18*, 1401–1407.
[4] a) A. S. Kumar, P. Gayathri, P. Barathi, R. Vijayaraghavan, *J. Phys. Chem. C* **2012**, *116*, 23692–23703; b) E. Nossol, A. J. G. Zarbin, *Adv. Funct. Mater.* **2009**, *19*, 3980–3986; c) S. Boopathi, S. S. Kumar, J. Joseph, K. L. Phani, *Electrochem. Commun.* **2011**, *13*, 294–297.
[5] H. Wei, E. Wang, *Anal. Chem.* **2008**, *80*, 2250–2254.
[6] a) F. Wang, Y. X. Ci, *Analyst* **1991**, *116*, 297–299; b) C. Wang, R. Yuan, Y. Chai, S. Chen, Y. Zhang, F. Hu, M. Zhang, *Electrochim. Acta* **2012**, *62*, 109–115; c) X. M. Huang, M. Zhu, L.-Y. Mao, H.-X. Shen, *Anal Sci* **1997**, *13*, 145–147; d) H. Liu, L. Zhang, J. Zhang, D. Ghosh, J. Jung, B. W. Downing, E. Whittemore, *J. Power Sources* **2006**, *161*, 743–752.
[7] a) Y. Zhang, Z. Xia, H. Liu, M. Yang, L. Lin, Q. Li, *Sens. Actuators* **2013**, *188*, 496–501; b) Z. Liu, R. Cai, L. Mao, H. Huang, W. Ma, *Analyst* **1999**, *124*, 173–176; c) T. Itoh, K. Yano, T. Kajino, Y. Inada, Y. Fukushima, *Biotechnol. Bioeng.* **2006**, *93*, 476–484; d) F. Valentini, L. Cristofanelli, M. Carbone, G. Palleschi, *Electrochim. Acta* **2012**, *63*, 37–46.
[8] a) B. Tang, M. Du, Y. Sun, H. L. Xu, H. X. Shen, *Talanta* **1998**, *47*, 361–366; b) C. Xia, X. Yanjun, W. Ning, *Electrochim. Acta* **2012**, *59*, 81–85; c) Y. Song, Z. He, H. Hou, X. Wang, L. Wang, *Electrochim. Acta* **2012**, *71*, 58–65; d) Z. Genfa, P. K. Dasgupta, *Anal. Chem.* **1992**, *64*, 517–522.
[9] a) A. A. Karyakin, E. E. Karyakina, L. Gorton, *Anal. Chem.* **2000**, *72*, 1720–1723; b) L. C. Chen, K. C. Ho, *Sens. Actuators, B* **2008**, *130*, 418–424; c) J. Y. Liu, X. F. Li, Z. X. Guo, Y. Z. Li, A. J. Huang, W. B. Chang, *J Mol Catal A Chem.* **2002**, *179*, 27–33; d) Z. Dai, S. Liu, J. Bao, H. Ju, *Chem. Eur. J.* **2009**, *15*, 4321–4326; e) S. K. Majia, A. K. Duttaa, P. Biswasa, D. N. Srivastavab, P. Paulb, A. Mondala, B. Adhikary, *Appl Catal A-Gen* **2012**, *419*, 170–177.
[10] a) S. Cosnier, C. Gondran, R. Wessel, F.-P. Montforts, M. Wedel, *Sensors* **2003**, *3*, 213–222; b) W. J. R. Santos, A. L. Sousa, R. C. S. Luz, F. S. Damos, L. T. Kubota, A. A. Tanaka, S. M. C. N. Tanaka, *Talanta* **2006**, *70*, 588–594; c) F. S. Damos, M. P. T. Sotomayor, L. T. Kubota, S. M. C. N. Tanaka, A. A. Tanaka, *Analyst* **2003**, *128*, 255–259.
[11] a) S. S. L. Castro, V. R. Balbo, P. J. S. Barbeira, N. R. Stradiotto, *Talanta* **2001**, *55*, 249–254; b) I. L. Mattos, L. Gorton, T. Ruzgas, *Biosens. Bioelectron.* **2003**, *18*, 193–200; c) K. C. Ho, C. Y. Chen, H. C. Hsu, L. C. Chen, S. C. Shiesh, X. Z. Lin, *Biosens. Bioelectron.* **2004**, *20*, 3–8; d) U. Scharf, E. W. Grabner, *Electrochim. Acta* **1996**, *41*, 233–239.
[12] S. Chakraborty, C. R. Raj, *J. Electroanal. Chem.* **2007**, *609*, 155–162.
[13] a) M. Ayala, R. Roman, R. Vazquez-Duhalt, *Biochem. Biophys. Res. Commun.* **2007**, *357*, 804–808; b) H. Yamada, R. Makino, I. Yamazaki, *Arch. Biochem. Biophys.* **1975**, *169*, 344–353.
[14] C. Gómez-Navarro, R. T. Weitz, A. M. Bittner, M. Scolari, A. Mews, M. Burghard, K. Kern, *Nano Lett.* **2007**, *7*, 3499–3503.
[15] a) S. C. Bhatia, N. Ravi, *Biomacromolecules* **2003**, *4*, 723–727; b) S. C. Bhatia, N. Ravi, *Biomacromolecules* **2000**, *1*, 413.
[16] a) J.-M. Zen, A. S. Kumar, M.-R. Chang, *Electrochim. Acta* **2000**, *45*, 1691–1699; b) M. F. S. Teixeira, F. H. Cincotto, P. A. Raymundo-Pereira, *Electrochim. Acta* **2011**, *56*, 6804–6811.
[17] H. Chen, S. Dong, *Biosens. Bioelectron.* **2007**, *22*, 1811–1815.
[18] a) A. S. Kumar, J.-M. Zen, *Electroanalysis* **2002**, *14*, 671–678; b) A. S. Kumar, P. Swetha, *J. Electroanal. Chem.* **2010**, *642*, 135–142; c) A. S. Kumar, P. Barathi, K. C. Pillai, *Colloids Surf. A* **2012**, *395*, 207–216.
[19] a) H. Zhao, Q. Sheng, J. Zheng, *Microchim. Acta* **2012**, *176*, 177–184; b) J. Wang, M. Gu, J. Di, Y. Gao, Y. Wu, Y. Tu, *Bioprocess Biosyst. Eng.* **2007**, *30*, 289–296.
[20] K. Yamamoto, G. Shi, T. Zhou, F. Xu, J. Xu, T. Kato, J. Y. Jin, L. Jin, *Analyst* **2003**, *128*, 249–254.
[21] S. Nellaiappan, A. S. Kumar, *Electrochim. Acta* **2013**, *109*, 59–66.

Received: August 3, 2013
Published online: November 6, 2013

